The supergene origin of ruthenian hexaferrum in Ni-laterites

(running head title: The supergene origin of ruthenian hexaferrum in Ni-laterites)

Thomas Aiglsperger[a,*], Joaquín A. Proenza[a], Salvador Galí[a], Jordi Rius[b], Francisco Longo[d], Cristina Domènech[a]

[a] *Departament de Mineralogia, Petrologia i Geologia Aplicada, Facultat de Ciències de la Terra, Universitat de Barcelona (UB), Martí i Franquès s/n, 08028 Barcelona, Spain*

**Corresponding author, e-mail: thomas.aiglsperger@ub.edu*

[b] *Institut de Ciència de Materials de Barcelona, CSIC, Campus de la Universitat Autònoma de Barcelona, Bellaterra, 08193 Barcelona, Spain*

[c] *Faculty of Engineering, Universidad Catolica Tecnologica del Cibao (UCATECI), Ave. Universitaria, esq. Ave. Pedro Rivera, PO Box 401, La Vega, Dominican Republic*

ABSTRACT

For two decades the nature of Fe-rich, oxygen-bearing, Ru-Os compounds found in the supergene environment has been debated. Ru-Os-Fe-oxides and nano-intergrowths of ruthenium with magnetite have been proposed. We have applied FE-SEM, EMPA, µ-Raman spectroscopy and synchrotron tts- µXRD to Ru-Os-Fe compounds recovered from Ni-laterites from the Dominican Republic. The results demonstrate that a significant portion of Fe exists in a common structure with the Ru-Os alloy, that is, ruthenian hexaferrum. This mineral occurs both as nanoparticles and as micrometric patches within a matrix of Fe-oxide(s). Our data suggest that supergene ruthenian hexaferrum with a

Suprimit: Supergenic
Suprimit: Ni laterite
Suprimit: unreveled
Suprimit: S
Suprimit:

Suprimit: Since
Suprimit: true
Suprimit: Fe
Suprimit: oxygen
Suprimit: is an unsolved problem
Suprimit: Fe oxide
Suprimit: vs.
Suprimit: In this contribution we
Suprimit:
Suprimit: We
Suprimit: is bound
Suprimit: to
Suprimit: ,
Suprimit: thus proving the true existence of
Suprimit:
Suprimit: Ruthenian hexaferrum
Suprimit: Fe oxide
Suprimit: It is believed that s

$(Ru_{0.4}(Os,Ir)_{0.1}Fe_{0.5})_{\Sigma 1.0}$ stoichiometry represents the most advanced weathering product of primary laurite within Ni-laterites from the Dominican Republic.

Introduction

Mineralogical investigation of micrometric platinum-group minerals (PGM) is essentially a question of analytical resolution. Fe-rich, oxygen-bearing, Ru-Os compounds from the weathered chromitite of the Vourinos complex (Greece) were first described by Garuti and Zaccarini (1997). However, at that time it was not possible to establish if these minerals were oxide compounds of platinum-group elements (PGE) or nano-intergrowth of Ru-rich alloy with Fe-oxide(s). Several authors reported PGM of similar composition from other localities around the world (e.g. Proenza et al. 2007; Uysal et al. 2009; Kapsiotis et al. 2011; González-Jiménez et al. 2014; O'Driscoll and González-Jiménez, 2016). The nature of these compounds has, nonetheless, remained uncertain. Recently, Zaccarini et al. (2014) analysed two Fe-rich and oxygen-containing Ru-Os compounds found in chromitites from Loma Peguera (Dominican Republic) using X-ray computed tomography and X-ray diffraction. They concluded that these grains consisted of "a fine intergrown of ruthenium and magnetite not detectable at the scale of the electron microprobe" and that desulphurization of primary PGM (e.g. laurite) formed porous grains of ruthenium, which were subsequently filled up by oxidizing fluids enriched in Fe, leading to crystallization of magnetite in cavities of the ruthenium grains during low temperature alteration. However, this interpretation assumes *ab initio* that PGE are inert during weathering of hypogene PGM, thus precluding any possible PGM transformation via Fe incorporation during lateritization. On the contrary, several authors suggested that PGE are mobile during

Suprimit: final alteration
Suprimit: hypogene PGE sulphides (e.g.
Suprimit:)
Suprimit: Ni laterite
Suprimit:
Suprimit: mostly
Suprimit: The first description on
Suprimit:
Suprimit:
Suprimit: was published
Suprimit: this
Suprimit: true
Suprimit:
Suprimit: oxides
Suprimit: -
Suprimit:
Suprimit: platinum group minerals (
Suprimit:)
Suprimit: with
Suprimit: ,
Suprimit: however, t
Suprimit: true nature of these compounds
Suprimit: ,
Suprimit: using X-ray computed tomography and X-ray diffraction,
Suprimit:
Suprimit:
Suprimit:
Suprimit: supergenic
Suprimit: alteration
Suprimit: the
Suprimit: might be

weathering (Bowles et al. 1986; McDonald et al. 1999; Melcher et al. 2005; Cabral et al. 2008; Garuti et al. 2012; Oberthür et al. 2014 and references therein). This contribution demonstrates, using innovative techniques for mineral microanalysis, that laurite is transformed to ruthenian hexaferrum at the low temperatures of lateritization.

Sample material and methods

Samples were collected in the Falcondo Ni-laterite mining area, which is located in the central part of the Dominican Republic (Fig. 1). From bottom to top, the weathering profile of this deposit is divided into: (i) serpentinized protolith (harzburgite>dunite>lherzolite), (ii) saprolite with hydrous Mg silicate-dominated mineralogy and (iii) limonite with Fe-oxide(s)-dominated mineralogy (Lewis et al. 2006; Tauler et al. 2009; Villanova de Benavent et al. 2014, 2016; Aiglsperger et al. 2016). Small chromitite occurrences without economic significance are scattered within the lateritic profile (Baurier-Aymat et al. 2015). Two PGE-rich chromitite samples were selected for this study: (i) one comes from the Loma Peguera ore deposit, containing ~3 ppm total PGE, and situated within saprolite (beneath the Mg-discontinuity) (Proenza et al. 2007; Aiglsperger et al. 2015), and (ii) the other, recovered from the Loma Larga ore deposit, represents a highly weathered chromitite body included in limonite (above the Mg-discontinuity). The latter sample is characterized by high PGE concentrations, up to 17.5 ppm total PGE (Fig. 2). Whole-rock PGE contents were obtained at Genalysis Ltd., Maddington, Western Australia, by ICP-MS after nickel sulphide fire assay collection, following the method described by Chan and Finch (2001). Detection limits are 1 ppb for Rh, and 2 ppb for Os, Ir, Ru, Pt and Pd. Both chromitite

Suprimit: 1994

Suprimit: Oberthuer

Suprimit:

Suprimit: will

Suprimit: Our results are twofold as they demonstrate the mobility of PGE in low temperature systems and provide evidence of Fe incorporation in Ru-Os compounds.

Formatat: Marca

Suprimit: Ni laterite

Suprimit: -

Suprimit:

Suprimit:

Suprimit: Scarce, s

Suprimit: ,

Suprimit:

Suprimit: given horizons of

Suprimit:

Suprimit: Mg-discontinuity

Suprimit: another one

Suprimit: hosting

Suprimit: Mg-discontinuity

Suprimit: which

Comentat [CD1]: no se ver las altas concentraciones de PGE en la fig.2

Suprimit: extremely

Suprimit: (

Suprimit:)

Suprimit: (

Suprimit:)

Suprimit:

Suprimit: (detection limits: 1 ppb for Rh, and 2 ppb for Os, Ir, Ru, Pt and Pd)

Suprimit: sulfide

samples, ~100 g each, were carefully crushed, milled and hand-sieved before processing by means of hydroseparation (HS) techniques at the HS laboratory Barcelona (Aiglsperger et al. 2015 and references therein). Heavy-mineral concentrates were mounted as polished, monolayer resin blocks and subsequently investigated by reflected-light microscopy and by scanning-electron microscopy (SEM) using a standard Quanta 200 FEI XTE 325/D8395, and a field-emission scanning-electron microscope (FE-SEM) Jeol JSM-7100 at the Serveis Científics i Tecnològics, University of Barcelona, Spain. At the same institution, PGE grains of interest were further investigated by element-distribution maps using a JEOL JXA-8230 electron microprobe (EMP) with an accelerating voltage of 20 kV and a beam current of 128.8 nA. Maps were collected by beam scanning with dwell times of 60 ms/pixel. For each element, the background map was subtracted from the corresponding peak map. Quantitative EMP analyses were obtained with the same instrument in the wavelength-dispersive spectroscopy (WDS) mode, operating with an accelerating voltage of 20 kV, a beam current of 10 nA and a beam diameter of 1 μm. Native elements were used as standards for Os, Ir, Ru, Rh, Pt, Pd, Co, Sb and S as well as chromite for Al and Fe, periclase for Mg, NiO for Ni, GaAs for As and wollastonite for Si. The following interferences RuLβ → RhLα, RhLβ → PdLα, RuLβ → PdLα and RhLα → PtLα were online-corrected.

Micro Raman maps were obtained by using a Thermo Scientific™ DXR™xi Raman imaging microscope. Areas were mapped at a laser power of 2 mW, the exposure time was 1 s with 5 scans and the pixel size was 1 μm. The raw data were treated with Thermo Scientific OMNIC™xi Raman imaging software.

Suprimit: (
Suprimit:)
Suprimit: processed
Suprimit: Heavy
Suprimit: optical reflected
Suprimit:
Suprimit: as well as
Suprimit: field
Suprimit: scanning
Suprimit: element
Suprimit: electron
Suprimit: microprobe
Suprimit: Pure metals
Suprimit: and
Suprimit: (
Suprimit: ,
Suprimit:)
Suprimit: (
Suprimit:)
Suprimit: (
Suprimit:)
Suprimit: S (S),
Suprimit: (
Suprimit:)
Suprimit: (
Suprimit:)
Suprimit: achieved
Suprimit: ec
Suprimit: Obtained

Synchrotron through-the-substrate X-ray microdiffraction (tts- µXRD) was used for the structural characterisation of crystalline mineral phases *in situ*, within standard polished thin sections (Rius et al. 2011, 2015). PGM-bearing monolayer polished sections were first transformed to polished thin sections, 30 µm thick, attached to an approximately <1 mm thick glass substrate. Subsequently, X-ray diffraction was carried out by both rotating and static thin sections. Experimental conditions were as follows: transmission mode, beam diameter of 30 µm, wavelength of 0.4325 Å, distance to a 2048×2048 pixel (79×79 µm^2) CCD detector of 190 mm. The intensities, as a function of the 2θ-diffraction angle, were obtained by integration of the complete Debye rings, between 0 and 23° (2θ), using the software Fit2d (Hammersley 1998; Dinnebier 2004). Diffraction profiles were further analysed and refined by the Rietveld method, using the Bruker software TOPAS Version 4.0 (TOPAS, 2009). The diffraction experiments were performed on the MSPD beamline at the ALBA Synchrotron Facility_CELLS, Cerdanyola,Barcelona, Spain.

Mineralogy of Fe-rich, oxygen-bearing, Ru-Os compounds

About 300 PGM grains with either Ru-, Ir- or Pt-dominant compositions were recovered; 125 grains of Ru-Os-Fe-bearing PGM, from ~10 to ~125 µm across, were selected from heavy-mineral concentrates from Loma Larga, as well as four Ru-Os-Fe compounds from Loma Peguera for comparison with literature data. Ru-Os-Fe-bearing PGM display diverse morphologies, from euhedral crystals to anhedral, rounded grains. They appear yellowish grey in reflected light microscopy and show strong anisotropy. BSE images of these grains reveal complex internal structures (see for example Fig. 3a of an imaged Ru-Os-Fe grain

Formatat: Tipus de lletra: No Cursiva

Suprimit:

Suprimit: (

Suprimit:)

Suprimit: the

Suprimit:

Suprimit: information

Suprimit: obtained

Suprimit: samples

Suprimit: The conditions of the experiment were

Suprimit: 30 µm

Suprimit: λ(Å)

Suprimit: 2θ

Suprimit: (

Suprimit:)

Suprimit: Fe

Suprimit:

Suprimit: A total of ~

Suprimit: dominated

Suprimit: mineralogy

Suprimit: from the processed chromitites

Suprimit:

Suprimit: ranging

Suprimit: in diameter

Suprimit: heavy

Suprimit: Fe

Suprimit: do not

Suprimit: (see for example Fig. 3a of an imaged Ru-Os-Fe grain from Loma Larga)

Suprimit:

from Loma Larga). They are characterized by (i) meandering banding at borders resembling erosion pits with subsequent infill, (ii) bright grey, irregularly formed, compact patches (up to 10 µm × 10 µm) and (iii) dark grey matrix material of high porosity. Quantitative element mapping by EMPA reveals different distribution patterns for the major elements Ru, Os and Fe (Fig. 3b-d): bright areas in BSE images correspond to the highest concentrations of Ru, which occur within compact patches as well as in bandings and in void infills at the border of the grain (Fig. 3b). On the other hand, Os appears mainly homogenously distributed with deficits in the central part of the grain (Fig. 3c). Fe shows highest concentrations within compact patches and close to the centre of the grain, where its distribution resembles a fine-structured network (Fig. 3d). In addition, Fe contributes to the Ru-rich banding at the border of the grain. However, element distribution mapping suggests that zones rich in Fe are depleted in Os, an observation that is supported by quantitative surface plots for the zone indicated in Fig. 3a, as well as by column average plots for the same area (Fig. 3e-g and 4, respectively). EMPA analyses (n=10) show that this complex microstructure corresponds to a very heterogeneous composition (Table 1). Highest totals close to 100 wt.% with a stoichiometry of $(Ru_{0.4}(Os,Ir)_{0.1}Fe_{0.5})_{\Sigma 1.0}$ are measured on compact patches (i.e. points 4 and 7 in Fig. 3a), whereas low totals (~90 wt.%) are observed within the fine-grained matrix material (e.g. points 2 and 10 in Fig. 3a). For comparison Ru-Os-Fe grains from Loma Larga (n=125) and from Loma Peguera (n=4) were quantified via EMP and plotted as at.% in a Ru-Os-Fe ternary diagram together with data from the literature. As can be seen in Fig. 5, Ru-Os-Fe grains from Loma Peguera plot close to results published by Zaccarini et al. (2014), whereas compositions of Ru-Os-Fe grains from Loma Larga reveal a clear Fe-enrichment trend towards the field of ruthenian hexaferrum (Mochalov et al. 1998).

Suprimit: of dense quality

Suprimit: porous

Suprimit: quality

Suprimit: EMPA analyses (n=10) show that this complex microstructure matches with heterogeneous composition (average and minimum - maximum in wt.%): Os 20 (16-23), Ir 9 (7-11), Ru 37 (25-46), Rh 0.07 (bdl-0.2), Pt 0.1 (bdl-0.4), Pd 0.05 (bdl-0.1), Fe 26 (23-30), Co 0.3 (0.1-0.4), Ni 0.5 (0.4-0.7), Sb 0.03 (bdl-0.07), S 0.07 (0.02-0.23), As 0.5 (0.4-0.7), Si 0.2 (0.01-0.3), Mg 0.04 (bdl-0.06), Al 0.4 (0.1-0.8), corresponding to an average total of 94 wt.% ranging from 89-101 wt.% (Table 1). Highest totals close to 100 wt.% with a stoichiometry of $(Ru_{0.4}(Os,Ir)_{0.1}Fe_{0.5})_{\Sigma 1.0}$ are measured on patches with a dense quality (i.e. points 4 and 7 in Fig. 3a) whereas lowest totals (~90 wt.%) are observed within the fine-grained matrix material (e.g. points 2 and 10 in Fig. 3a).

Suprimit: s

Suprimit: of dense quality

Suprimit: osmium

Suprimit: of dense quality

Suprimit: braiding

Suprimit: Ru

Suprimit: s

Suprimit: which

Formatat: No Marca

Comentat [CD2]: el punto es necesario?

Formatat: No Marca

Formatat: No Marca

The same area as for quantitative surface plots was used for a detailed μ-Raman spectroscopy investigation and maps obtained revealed the presence of at least three mineral compounds: (i) one Raman inactive mineral, (ii) one mineral with its main bands at 667 and 720 cm^{-1} and (iii) one mineral with its main bands at 226, 300, 410 and 1325 cm^{-1} (Fig. 6). The Raman inactive mineral is associated with the bright-appearing compact patches and highest Ru concentrations (e.g. point 7 in Fig. 3a), whereas Raman active minerals are associated with the dark-appearing, Fe-rich matrix material (Fig. 6 a-c). Comparison with literature data shows that Raman active minerals are Fe-oxide(s) with best fits for maghemite and hematite. Furthermore, Fe-oxide(s)-rich zones in Raman maps resemble micro channels circuiting Raman inactive, Ru-rich compounds (Fig. 6c).

Suprimit: 5
Suprimit: bright
Suprimit: of dense quality
Suprimit: dark
Suprimit: Fe
Suprimit: 5
Suprimit: Fe
Suprimit: a
Suprimit: However, shapes of Fe oxide
Suprimit:)
Suprimit:

Synchrotron tts- μXRD of the same grain revealed the presence of two mineral phases: one belonging to the isometric (cubic) structure and one mineral belonging to the hexagonal structure (space group $P6_3/mmc$). Assessments of diffraction patterns of the isometric mineral confirmed the presence of Fe-rich spinel ($d_{(111)} = 4.76$ Å and $d_{(220)} = 2.92$ Å) Subsequently, d_{hkl} values and cell parameters of the hexagonal compound were compared to relevant literature data (Table 2 and 3), which led to the identification of ruthenian hexaferrum (Mochalov et al. 1998) with cell parameters of $a = 2.664(1)$ Å and $c = 4.250(2)$ Å. The analysis of the diffraction profile, compared with the instrumental profile of the experiment obtained with a conventional standard of LaB6, allowed the estimation of the diffracting domains of ruthenian hexaferrum averaged over volume Lvol = 28 nm. The particles are estimated to be essentially free from strain ($\varepsilon 0 = 0.025$) (Balzar, 1999). Figure 7 depicts the experimental, calculated and difference profiles.

Suprimit: oxidized magnetite
Formatat: Marca
Suprimit: , which is in good agreement with the μ-Raman data
Suprimit:
Suprimit:
Suprimit: In f
Suprimit: 6
Suprimit: are depicted

Supergene formation of ruthenian hexaferrum in Ni-laterites

Synchrotron tts- µXRD data confirm that a significant proportion of Fe is bound to the Ru and Os suggesting that Fe-rich Ru-Os grains are mainly composed of accumulations of nano-sized ruthenian hexaferrum. The aggregation of these nanoparticles can produce larger, compact patches as observed in high-resolution FE-SEM BSE images (Fig. 8). Previous work has shown that hypogene PGM (e.g. laurite) can transform during serpentinization to secondary PGM hosting Mg silicate on a sub-micron scale (e.g. Uysal et al., 2009). FE-SEM images and energy-dispersive X-ray spectroscopy (EDS) analyses of Ru-Os alloys included in chromite suggest that serpentinization results in (i) desulphurization of the primary laurite and (ii) nanoscaled intergrowth of Mg silicates with Ru-Os alloys (Fig. 9). However, these Mg silicates are not stable within higher levels of the Ni-laterite (close to the Mg discontinuity), hence weathering of Mg silicates results in a significant increase of porosity and permeability within the Ru-Os alloy. As a consequence, oxidized, Fe-rich fluids can enter the grain along micro channels and crystallize as Fe-oxide(s) (Zammit et al. 2015). According to synchrotron µ-XRD analysis and µ-Raman spectroscopy, Fe-oxide(s) observed within the studied PGM are maghemite and trace amounts of hematite, which exhibit a close spatial relationship with ruthenian hexaferrum nanoparticles (Fig. 6 and 8). Barrón and Torrent (2002) showed that maghemite may form in tropical soils as a transient phase during the transformation of ferrihydrite to hematite. Transformation processes of nanoscaled Fe-oxide(s) within the highest levels of the Ni-laterite profile may explain the observed Fe incorporation into Ru-Os alloys. Alternatively,

Suprimit: Ni laterite
Suprimit: Fe
Suprimit: of dense quality
Suprimit: 7
Suprimit: ,
Suprimit: -
Suprimit: s
Suprimit: can be incorporated in hypogene PGM (e.g. laurite)
Suprimit: at serpentinization stage on a sub-micron scale
Suprimit: ; McDonald et al., 2010 and reference therein
Formatat: Marca
Suprimit: PGM
Suprimit: , (ii) significant redistribution of PGE
Suprimit: i
Suprimit: -
Suprimit: PGE
Suprimit: 8
Suprimit: -
Suprimit: Ni laterite
Suprimit: -
Suprimit: to
Suprimit: PGE
Suprimit:
Suprimit: Fe oxide
Suprimit: and synchrotron µ-XRD analysis here observed Fe oxide
Suprimit: most likely oxidized magnetite,
Formatat: No Marca
Suprimit: (Fig. 5),
Suprimit: 7
Suprimit: with hexagonal closest packing
Suprimit: Fe oxide
Suprimit: Ni laterite
Suprimit: here

magnetite could have first crystallized during early stages of lateritization within porous Ru-Os alloys and was then subsequently oxidized to maghemite. Recent studies suggest that at latest stages of lateritization, maghemite is transformed to goethite via biogenic mediated dissolution-reprecipitation processes that imply the availability of Fe^{2+} ions (Monteiro et al. 2014). According to preliminary thermodynamic calculations, a Fe-Ru alloy would be unstable with regards to Ru(0) and aqueous Fe^{2+}. However, catalytic effects of the fine-grained and porous Ru(0) grain texture may favour the formation of a metastable Ru-Fe alloy (i.e. ruthenian hexaferrum), which can coexist with magnetite and/or goethite at circumneutral pH (Fig. 10). The oxidizing conditions with expected remobilization of PGE (Ru>Os) at low pH due organic acids and high Eh conditions most likely favour the formation and subsequent accumulation of ruthenian hexaferrum nanoparticles at the Ru-Os alloy – Fe-oxide(s) interface as indicated by (i) banding features at the grain´s boundary and (ii) formation of patches (Fig 8).

Fig. 11 summaries the proposed model of supergene hexaferrum formation within Ni-laterites.

Conclusions

Our observations and data suggest that supergene ruthenian hexaferrum with a $(Ru_{0.4}(Os,Ir)_{0.1}Fe_{0.5})_{\Sigma 1.0}$ stoichiometry marks the final product of laurite alteration in Ni laterites from Falcondo.

Supergene ruthenian hexaferrum is believed to form via (i) desulphurization of primary laurite with subsequent Mg silicate incorporation into the fine-grained Ru-Os alloy during

Suprimit: A

Suprimit: believed to be

Suprimit: which

Suprimit: ,

Suprimit: data

Suprimit:

Comentat [CD3]: Te envié una nueva version de la figura donde el Fe(cr) está escrito como Fe(0). Así estará con más coherencia en el texto. Por favor, utiliza ésta.

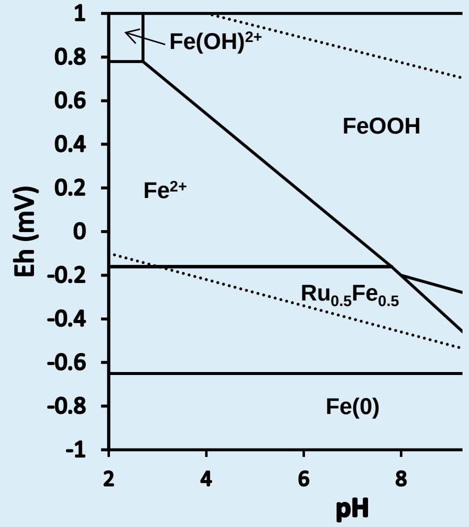

Suprimit: 9

Suprimit: Fe oxide

Comentat [CD4]: ATENCION QUE SEGÚN EL DIAGRAMA SOLO COEXISTEN GOETHITA CON MAGNETITA CON HEXAFERRUM A Ph ...

Comentat [CD5]: Pero si que es cierto que estas condiciones son más oxidantes y ácidas que las que se esperan en las serpentinas. ...

Comentat [CD6]: Pero si yo tuviera que dar un valor a un pH ácido y a un Eh oxidante no serian ni 7.5 ni 0 V respectivamente.

Comentat [CD7]: He revisado antiguas versiones y también estaba así con lo que lo que digo no sé si tiene mucho sentido. ...

Suprimit: porosity reduction (

Suprimit:)

Suprimit: 7

Suprimit: hypogenePGM (e.g.

Suprimit:)

Suprimit: (Fig 10)

Suprimit:

Suprimit: PGM (e.g. laurite)

Suprimit: Mg-silicate

serpentinization, followed by (ii) weathering of Mg silicates within the Ru-Os alloy at high levels of the Ni-laterite profile (above the Mg-discontinuity) and subsequently by (iii) crystallization of Fe-oxide(s) within highly porous Ru-Os alloy and finally, (iv) transformation of magnetite or ferrihydrite to hematite via maghemite, causing Fe incorporation into the Ru-Os alloy.

Acknowledgements

This research has been financially supported by FEDER Funds, the Spanish projects CGL2012-36263 and CGL2015-65824 and the Catalan project 2014-SGR-1661 as well as by a PhD grant to TA sponsored by the Ministerio de Economía y Competitividad (Spain). The authors gratefully acknowledge the help and hospitality extended by the staff of Falcondo mine (Falcondo Glencore). Excellent technical support during EPMA sessions by Dr. X. Llovet and during FESEM sessions by Eva Prats at the Serveis Científics i Tecnòlogics (University of Barcelona) is highly appreciated. Louis Cabri and Vladimir Rudashevsky are greatly thanked for their help during installation of the HS-11 laboratory in Barcelona. Many thanks to the stuff of the ALBA Synchrotron Facility_CELLS. Insightful comments and stimulating discussion with José María González Jiménez have improved this work. We acknowledge the constructive criticism of Dr. John Bowles, Dr. Alexandre Cabral and Dr. Louis J. Cabri as well as the help of the scientific editor of Terra Nova, Prof. Georges Calas. The authors declare that no conflict of interest exists.

Figure captions

Suprimit: -

Suprimit: Ni laterite

Suprimit: Mg-discontinuity

Suprimit: , followed

Suprimit: Fe oxide

Suprimit: processes of Fe oxide(s) (

Suprimit:)

Suprimit: subsequent

Suprimit: of Fe

Suprimit: Organic acids and high Eh conditions at highest levels of the Ni laterite profile are believed to favour *in situ* neoformation of ruthenian hexaferrum nanoparticles.

Suprimit: Constructive discussions

Suprimit: ¶

Suprimit: ¶

Suprimit: ¶

Fig. 1 A) Geographic location of the Loma Caribe peridotite and orthophotograph of the Falcondo mining area highlighting the Loma Larga and Loma Peguera ore deposits. B) simplified geological map of the central section of the Loma Caribe peridotite (modified from Bowin 1966; Escuder-Viruete et al. 2007).

Fig. 2 Idealized Ni-laterite soil profile from the Falcondo mining area showing different zones and variation in chemical composition. The location of PGM rich chromitites within saprolite (beneath the Mg-discontinuity) and limonite (above the Mg-discontinuity) is indicated.

Suprimit: Ni laterite

Suprimit: Mg-discontinuity

Suprimit: Mg-discontinuity

Fig. 3 BSE image of one representative Fe rich, oxygen bearing, Ru-Os grain with indicated points of EMP measurements, zone of surface plots and profile direction a-b for column average plots (A); quantitative element mappings for Ru, Os and Fe (B-D); surface plots of marked area in (A) for Ru, Os and Fe with indicated profile direction a-b for column average plots (E-G).

Fig. 4 Ru, Fe and Os concentrations of column average plots along the rectangle from a-b as indicated in Fig. 3a.

Fig. 5 Ternary diagram in the Os-Fe-Ru system showing the compositional transforamtion trend from Ru-rich alloys towards ruthenian hexaferrum. Note: Fe enrichment is mainly explained by formation of ruthenian hexaferrum. Compositional fields reproduced from Mochalow et al. (1998).

Fig. 6 Micro Raman spectroscopy mapping of the Ru-Os-Fe grain (A-C) with reference spectra for common Fe-oxide(s) (modified from Froment et al. 2008) (D).

Suprimit: Fe oxide

Fig. 7 Comparison of observed synchrotron XRD pattern with calculated pattern for ruthenian hexaferrum (spectra have been shifted for clarity). Baseline refers to the difference of profiles. The Rietveld refinement of the profile was obtained by integration of Debye rings converged at an agreement index Rwp = 1.79.

Suprimit: 6

Formatat: Tipus de lletra per defecte del paràgraf

Fig. 8 FE-SEM BSE images showing the fine grained nature of one representative ruthenian hexaferrum grain: meandering Ru rich banding at the grain´s border resembling erosion pits with subsequent infill (A); accumulation of ruthenian hexaferrum nanoparticles (bright) within Fe-oxide(s) matrix (dark) (B); close-up of the interface between Fe-oxide(s) containing ruthenian hexaferrum nanoparticles (right) and a compact ruthenian hexaferrum patch (left) with indicated direction of ruthenian hexaferrum accumulation (C); close-up of one characteristic bright grey, irregularly formed, compact ruthenian hexaferrum patch (3µm × 3µm) (D).

Suprimit: 7

Suprimit: Fe oxide

Suprimit: close

Suprimit: Fe oxide

Suprimit: of dense quality

Suprimit: close

Suprimit: of dense quality

Suprimit: x

Fig. 9 Fine-grained, porous appearing Ru-Os alloy included between chromian spinel (right) and an Mg silicate vein (left). Note: no sulphur but significant amounts of Mg and Si are present in EDS spectra of the Ru-Os alloy.

Suprimit: 8

Suprimit: Mg-silicate

Fig. 10 Predominance diagram of the Fe-Ru-H_2O system at 25ºC and 1 atm drawn with the Medusa software Package (Puigdomenech 2010), assuming a $[Fe]_{total} = 10^{-7}$ M and $[Ru]_{total}=10^{-15}$ M. Ru(0) is not allowed to form. Thermodynamic data used for calculations

Suprimit: 9

Suprimit: .

Suprimit: Ru(0) is not allowed to form. $[Fe]_{total} = 10^{-7}$ M; $[Ru]_{total}=10^{-15}$ M.

include the following aqueous species, gas and solid phases: Fe^{2+}, Fe^{3+}, Ru^{2+}, Ru^{3+}, H^+, OH^-, H_2, $H_2(g)$, O_2, $O_2(g)$, H_2O, $Fe(OH)_2$, $Fe(OH)_3^-$, $Fe(OH)_4^{2-}$, $FeOH^+$, $Fe(OH)_2^+$, $Fe(OH)_3$, $Fe(OH)_4^-$, $Fe_2(OH)_2^{4+}$, $Fe_3(OH)_4^{5+}$, $FeOH^{2+}$, Fe(0), $Ru_{0.5}Fe_{0.5}$, Fe_3O_4 and FeOOH. Thermodynamic data for all aqueous species and solid phases, except those of Ru, come from Thermochimie v.9 database (Giffaut et al. 2014, https://www.thermochimie-tdb.com/). Due to limited thermodynamic data of Ru available in the literature two reactions have been included in the calculations, whose log K have been calculated from electrochemical data from literature.

$0.5Fe^{2+} + 0.5\ Ru^{2+} + 2e^- = Ru_{0.5}Fe_{0.5}$ logK=5.20 r.1

$Ru^{3+} + e^- = Ru^{2+}$ log K = 4.21 r.2

Fig. 11 Simplified model explaining the formation of supergene ruthenian hexaferrum via multiple stage alteration of primary laurite as a result of the geochemical evolution of the Ni-laterite profile.

Table captions

Table 1 Electron microprobe analyses of points indicated in Fig. 3a.

Table 2 Comparison of X-ray data for ruthenian hexaferrum of this study and chemically related phases; [a] McDonald et al. (2010).

Suprimit:

Suprimit:

Suprimit: , e^-.

Suprimit: :

Suprimit: r

Formatat: Justificada, Interlineat: Doble, Tabulacions: 8 cm, Esquerra

Suprimit:

Formatat: Tipus de lletra: 12 pt, alemany (Àustria)

Formatat: Tipus de lletra: 12 pt, alemany (Àustria)

Formatat: Tipus de lletra: 12 pt, Espanyol (Espanya)

Formatat: Espanyol (Espanya)

Suprimit:

Formatat: Tipus de lletra: 12 pt, Espanyol (Espanya)

Formatat: Espanyol (Espanya)

Formatat: Espanyol (Espanya)

Formatat: Tabulacions: 8 cm, Esquerra

Suprimit:

Formatat: Tipus de lletra: 12 pt, Espanyol (Espanya)

Formatat: Tipus de lletra: 12 pt, Espanyol (Espanya)

Formatat: Tipus de lletra: 12 pt, Espanyol (Espanya)

Formatat: Tipus de lletra: 12 pt, Espanyol (Espanya)

Suprimit: 10

Suprimit: Ternary diagram in the Os-Fe-Ru system showing the compositional transforamtion trend from primary laurite to ruthenian hexaferrum. Note: Fe enrichment is mainly explained by formation of ruthenian hexaferrum

Formatat: Superíndex

Table 3 Comparative data for ruthenian hexaferrum of this study with ruthenium and osmium-group mineral and garutiite.

References:

Aiglsperger, T., Proenza, J.A., Zaccarini, F., Lewis, J.F., Garuti, G., Labrador, M., Longo, F., 2015. Platinum group minerals (PGM) in the Falcondo Ni-laterite deposit, Loma Caribe peridotite (Dominican Republic). *Miner. Deposita*, **50**, 105-123.

Aiglsperger, T., Proenza, J.A., Lewis, J.F., Labrador, M., Svojtka, M., Rojas-Purón, A., Longo, F., Ďurišová, J., 2016. Critical metals (REE, Sc, PGE) in Ni-laterites from Cuba and the Dominican Republic. *Ore Geol. Rev.*, **73,** 127-147.

Arndt, U.W. and Wonacott, A.J., 1977. The Rotation Method in Crystallography. Amsterdam, *North Holland Biomedical Press*, Elsevier.

Balzar, D., 1999. Voigt-function model in diffraction line broadening analysis. In: *Microstructure Analysis from Diffraction*, edited by R.L. Snyder, H. J. Bunge and J. Fiala, *International Union of Crystallography*, 94-126.

Suprimit: Ni laterite

Suprimit: Ni laterite

Comentat [CD8]: No se cita

Barrón, V. and Torrent, J., 2002. Evidence for a simple pathway to maghemite in Earth and Mars soils. *Geochim. Cosmochim. Acta*, **66**, 2801-2806.

Baurier-Aymat, S., Aiglsperger, T., Proenza, J.A., Lewis, J.F., Longo, F., 2015. Chromian spinel composition, PGE geochemistry and PGE mineralogy of different chromitites from the Loma Caribe peridotite, Dominican Republic. *Proceedings of the 13th SGA Biennial Meeting (Nancy, France)*, **3**, 889-892.

Bowin, C.O., 1966. Geology of the central Dominican Republic (a case history of part of an island arc). In: Hess, H. (Ed.), Caribbean Geological Studies. *Mem. Geol. Soc. Am.*, **98**, 11-84.

Bowles, J.F.W. 1986. The development of platinum-group minerals in laterites. *Econ. Geol.*, **81**, 1278-1285.

Cabral, A.R., Galbiatti, H.F., Kwitko-Ribeiro, R., Lehmann, B., 2008. Platinum enrichment at low temperatures and related microstructures, with examples of hongshiite (PtCu) and empirical ‘Pt_2HgSe_3’ from Itabira, Minas Gerais, Brazil. *Terra Nova*, **20**, 32–37.

Chan, T.K. and Finch, I.J., 2001. Determination of platinum-group elements and gold by inductively coupled plasma mass spectrometry. In: Australian Platinum Conference, Perth, Western Australia, pp. 1-9.

Suprimit: Bowles, J.F.W., Gize, A.P., Vaughan, D.J., Norris, S.J., 1994. Development of platinum-group minerals in laterites-initial comparison of organic and inorganic controls. *Transact. Instn. Min. Metall.*, **103**, B53-B56.¶

Formatat: Tipus de lletra: Cursiva

Formatat: Tipus de lletra: Negreta

Suprimit: ¶

Dinnebier, R.E., 2004. Batch conversion from 2D to 1D powder diffraction data using Fit2D V12.043. *A short tutorial*. (copyright 1987-2004 Andy Hammersley/ESRF).

Escuder Viruete, J., Pérez-Estaún, A., Contreras, F., Joubert, M., Weis, D., Ullrich, T.D., Spadea, P., 2007. Plume mantle source heterogeneity through time: Insights from the Duarte Complex, Hispaniola, northeastern Caribbean. *J. Geophys. Res.*, **112**, B04203.

Froment, F., Tournié, A., Colomban, P., 2008. Raman identification of natural red to yellow pigments: ochre and iron-containing ores. *J. Raman Spectrosc.*, **39**, 560-568.

Garuti, G. and Zaccarini, F., 1997. In situ alteration of platinum-group minerals at low temperature: evidence from serpentinized and weathered chromitite of the Vourinos complex, Greece. *Can. Mineral.*, **35**, 611-626.

Garuti, G., Zaccarini, F., Proenza, J.A., Thalhammer, O.A.R., Angeli, N., 2012. Platinum-group minerals in chromitites of the Niquelândia layered intrusion (Central Goias, Brazil): Their magmatic origin and low-temperature reworking during serpentinization and lateritic weathering. *Minerals*, **2**, 365-384.

Giffaut, E., Grivé, M., Blanc, Ph., Vieillard, Ph., Colàs, E., Gailhanou, H., Gaboreau, S., Marty, N., Madé, B., Duro, L., 2014. Andra thermodynamic database for performance assessment: ThermoChimie. *Appl. Geochem.*, **49,** 225-236.

González-Jiménez, J.M., Griffin, W.L., Gervilla, F., Proenza, J.A., O'Reilly, S.Y., Pearson, N.J., 2014. Chromitites in ophiolites: how, where, when, why? Part I. Origin and significance of platinum-group minerals. *Lithos*, **189**, 127-139.

Hammersley, A.P., 1998. Fit2D: V99.129 Reference Manual Version 3.1. *Internal Report ESRF-98-HA01*.

Kapsiotis, A., Grammatikopoulos, T.A., Tsikouras, B., Hatzipanagiotou, K., Zaccarini, F., Garuti, G., 2011. Mineralogy, composition and PGM of chromitites from Pefki, Pindos Ophiolite Complex (NW Greece): evidence for progressively elevated fAs conditions in the upper mantle sequence. *Mineral. Petrol.*, **101**, 129-150.

Lewis, J.F., Draper, G., Proenza, J.A., Espaillat, J., Jiménez, J., 2006. Ophiolite-related ultramafic rocks (serpentinites) in the Caribbean region: a review of their occurrence, composition, origin, emplacement and nickel laterite soils. *Geol. Acta*, **4**, 237-263.

McDonald, A.M., Proenza, J.A., Zaccarini, Z., Rudashevsky, N.S., Cabri, L.J., Stanley, C.J., Rudashevsky, V.N., Melgarejo, J.C., Lewis, J.F., Longo, F., Bakker, R.J., 2010. Garutiite, (Ni,Fe,Ir), a new hexagonal polymorph of native Ni from Loma Peguera, Dominican Republic. *Eur. J. Mineral*, **22**, 293-304.

McDonald, I., Ohnenstetter, D., Ohnenstetter, M., Vaughan, D.G. 1999. Palladium oxides in ultra-mafic complexes near Lavatrafo, Western Andriamana, Madagascar. *Mineral. Mag.*, **63**, 345–352.

Melcher, F., Oberthür, T., Lodziak, J. 2005. Modification of detrital platinum-group minerals from the eastern Bushveld Complex, south Africa. *Can. Mineral.*, **43**, 1711–1734.

Mochalov, A.G., Dmitrenko, G.G., Rudashevsky, N.S., Zhernovsky, I.V., Boldyreva, M.M., 1998. Hexaferrum (Fe,Ru),(Fe,Os), (Fe,Ir) – a new mineral. Zap. Vseross. Mineral. Obshch. 127, 41–51 (in Russian).

Monteiro, H.S., Vasconcelos, P.M., Farley, K.A., Spier, C.A., Mello, C.L., 2014. (U–Th)/He geochronology of goethite and the origin and evolution of cangas. *Geochim. Cosmochim. Acta*, **131**, 267–289.

O'Driscoll, B., González-Jiménez, J., 2016. Petrogenesis of the platinum-group minerals. *Rev. Mineral. Geochem.*, **81**, 489–578.

Oberthür, T., Weiser, T.W., Melcher, F., 2014. Alluvial and Eluvial Platinum-group minerals from the Bushveld Complex, South Africa. *S. Afr. J. Geol.*, **117**, 255-274.

Proenza, J.A., Zaccarini, F., Lewis, J., Longo, F., Garuti, G., 2007. Chromian spinel composition and platinum-group mineral assemblage of PGE-rich Loma Peguera chromitites, Loma Caribe peridotite, Dominican Republic. *Can. Mineral.*, **45**, 211–228.

Puigdomènech, I., 2010. MEDUSA (Make Equilibrium Diagrams Using Sophisticated Algorithms) Windows interface to the MS-DOS versions of INPUT, SED and PREDOM (FORTRAN programs drawing chemical equilibrium diagrams) Version 6 Dec 2010. *Royal*

Formatat: anglès (EUA)

Suprimit: ¶

Formatat: Espanyol (Espanya)

Suprimit: ¶

Suprimit: Oberthuer

Institute of Technology, Stockholm, Sweden. https://sites.google.com/site/chemdiagr/download.

Rius, J., Labrador, A., Crespi, A., Frontera, C., Vallcorba, O., Melgarejo, J.C., 2011. Capabilities of through-the-substrate micro-diffraction: application of Patterson-function direct methods to synchrotron data from polished thin sections. *J. Synchrotron Rad.*, **18**, 891-898.

Rius, J., Vallcorba, O., Frontera, C., Inmaculada, P., Crespi, A., Miravitlles, C., 2015. Application of synchrotron through-the-substrate micro-diffraction to crystals in polished thin sections. *IUCrJ*, **2**, 452-463.

Falta Swanson et al. (1955)

Tauler, E., Proenza, J.A., Galí, S., Lewis, J.F., Labrador, M., García-Romero, E., Suárez, M., Longo, F., Bloise, G., 2009. Ni-sepiolite–falcondoite in garnierite mineralisation from the Falcondo Ni-laterite deposit, Dominican Republic. *Clay Miner.*, **44**, 435–454.

TOPAS, 2009. General Profile and Structure Analysis for Powder Diffraction Data, version 4.2, Bruker AXS, GmbH, Germany.

Falta Urashima et al. 1974 (table 3)

Comentat [CD9]:

Comentat [CD10]:

Formatat: Espanyol (Espanya)

Formatat: Espanyol (Espanya)

Uysal, I., Zaccarini, F., Sadiklar, M.B., Bernhardt, H.-J.M., Bigi, S., Garuti, G., 2009. Occurrence of rare Ru–Fe–Os–Ir–oxide and associated Platinum-group minerals (PGM) in the chromitite of Mugla ophiolite, SW-Turkey. *Neues Jahrbuch für Mineralogie (Abhandlungen)*, **185**, 323–333.

Villanova-de-Benavent, C., Proenza, J.A., Galí, S., García-Casco, A., Tauler, E., Lewis J.F., Longo, F., 2014. Garnierites and garnierites: Textures, mineralogy and geochemistry of garnierites in the Falcondo Ni-laterite deposit, Dominican Republic. *Ore Geol. Rev.*, **58**, 91-109.

Villanova-de-Benavent, C., Nieto, F., Viti, C., Proenza, J.A., Galí, S., Roqué-Rosell, J., 2016. Ni-phyllosilicates (garnierites) from the Falcondo Ni-laterite deposit (Dominican Republic): Mineralogy, nanotextures, and formation mechanisms by HRTEM and AEM. *Am. Mineral.*, **101**, 1460-1473.

Zaccarini, F., Bindi, L., Garuti, G., Proenza, J.A., 2014. Ruthenium and magnetite intergrowths from the Loma Peguera chromitite, Dominican Republic, and relevance to the debate over the existence of platinum-group element oxides and hydroxides. *Can. Mineral.*, **52**, 617–624.

Zammit, C.M., Shuster, J.P., Gagen, E.J., Southam, G., 2015. The geomicrobiology of supergene metal deposits. *Elements*, **11**, 337-342.

Formatat: Espanyol (Espanya)

Suprimit: Ni laterite